Orbital forcing of the Plio-Pleistocene Indian monsoons: benthic foraminiferal proxies from ODP Site 758

Anil K. Gupta[†,*] and Jean-Luc Mélice[#]

[†]Department of Geology and Geophysics, Indian Institute of Technology, Kharagpur 721 302, India
[#]Institut de Recherche pour le Développement, Laboratoire d'Océanographie Dynamique et de Climatologie, Université Pierre et Marie Curie, Paris, France

The Indian Ocean monsoon system is one of the dominant features of the earth's climate influencing weather and climate of the Asian region. Long-term changes in the monsoon have been linked to orbital forcings as well as the Himalayan–Tibetan uplift. Changes in the monsoon are preserved in various proxies across the region both on land and in the marine sediments. Here we present Plio-Pleistocene record of monsoon proxy deep-sea benthic foraminifera from Ocean Drilling Programme Site 758, northeast ern Indian Ocean to understand a link between orbital changes and Indian Ocean monsoon variability. We used Continuous Wavelet Transform (CWT) of *Uvigerina proboscidea* and *Epistominella exigua*, which have been found blooming in two different seasons of the Indian monsoon – the summer and winter monsoons, respectively. An inverse relation between the two is observed during the past ~1000 kyr in the CWT-extracted 400-kyr components as also in the raw data. The variable relation between the monsoon proxies and earth's eccentricity at Site 758 agrees with the recent findings that orbital forcing of the Indian monsoon shows major shifts during the Plio-Pleistocene. These shifts correspond to the advent of growth and decay of the Northern Hemisphere ice sheets since the last 2.5 Ma.

THE Indian Ocean climate is dominated by the summer or southwest (SW) monsoon and winter or northeast (NE) monsoon winds, affecting weather and climate of the Asian and African regions between 30°N and 20°S latitudes[1]. Winds are stronger and precipitation is high during the summer monsoon season, whereas during the winter monsoon months weak and variable winds cause low precipitation. Both sensible and latent heating drive the summer monsoon winds between the cold Indian Ocean and the warmer Indian–Asian land mass (Himalayan–Tibetan Plateau) during May–July[2]. During winter,

*For correspondence. (e-mail: anilg@gg.iitkgp.ernet.in)

northeast trades develop when the pressure gradients reverse and the land mass becomes colder than the oceans[3].

Most parts of the Indian subcontinent receive rain during the normal SW monsoon season, enhancing agricultural productivity in the region. But an unusual summer monsoon may bring floods and may cause droughts, affecting the daily life of people of the region. Thus the monsoon is an important aspect of socio-economic life of people of the subcontinent. Past changes in the monsoon circulation appear to have triggered migration of human population in the Indian subcontinent, leading to appearance and disappearance of various human civilizations[4]. The population response to the monsoon variability in the African region has recently been studied by de Menocal[5], who found a close relation between human migration and African aridity during the Plio-Pleistocene and in the Holocene. However, similar studies from the Indian subcontinent are few, although the monsoon variability is of great importance to the people of India.

The monsoon winds induce upwelling in the upper water column that controls oceanic primary productivity and promotes the blooming of distinct fauna and flora in different parts of the northern Indian Ocean. During winter, the biological production is mostly low, but in summer intense monsoonal circulation causes coastal and open-ocean upwelling that enhances the surface productivity[6,7]. The biological response to monsoonal activity in the surface water column is preserved in planktic foraminifera. Deep-sea benthic foraminifera, on the other hand, carry signatures of the total export flux of food to the sea floor and its seasonality[8–13]. We use these proxies to trace changes in the strength and seasonality of the monsoons.

Like other major components of climate, the SW Indian monsoon has varied at orbital periodicities (Milankovitch cycles) during the Plio-Pleistocene[7,14–17]. According to the Milankovitch theory, global climatic changes are induced by ice-volume fluctuations linked with oscillations of the 65°N summer solstice insolation. Some recent studies correlate the monsoon variability to the Northern Hemisphere climate (glacial–interglacial variability)[18]; therefore one would expect changes in the monsoon over the last 5 Ma as climate entered from warm to cool mode in the middle Pliocene[14,19]. Palaeoclimatic records show major phase changes in the Indian monsoon relative to insolation during the Plio-Pleistocene[14]. Orbital forcing of the Indian monsoon indicates that before 2.4 Ma the SW monsoon varied at precessional periodicity and after 2.4 Ma, the 41-kyr component shows increased variance[20]. The 100-kyr earth's eccentricity cycles began to dominate the SW monsoon variability since ~1.2 Ma (refs 14, 19). The 400-kyr component of earth's eccentricity shows increased variance in the SW monsoon at about 0.9 Ma (ref. 17). However, in the NE monsoon while the precession and obliquity signals are weak, the eccentricity (100-kyr) signal is stronger[13]. These shifts in the orbital cycles are also visible in the Plio-Pleistocene African climate[5]. In the present study we attempt to understand a link between orbital changes and summer as well as winter monsoon variability using deep-sea benthic foraminiferal proxy record from the Ocean Drilling Program (ODP) Site 758, northeastern Indian Ocean.

Materials and methods

We analysed 134 samples from ODP Site 758, using the age model in Peirce *et al.*[21] and updated it to the Berggren *et al.*[22] timescale. Core samples of 10 cc volume were processed using the standard procedures as described in Gupta and Thomas[12]. We generated benthic foraminiferal census data from an aliquot of ~300 specimens in the >125 μm size fraction. Located at 5°23.05′N lat and 90°21.67′E long at a water depth of 2924 m in the northeastern Indian Ocean below a divergence (Figure 1), Site 758 is the only site that lies under the influence of both the SW and NE Indian monsoons to the east of the Indian land mass[23]; thus this site offers a good complement to those from the Arabian Sea. The reversing monsoonal winds develop major divergences and convergences in the region (Figure 1), which control the surface primary productivity at Site 758.

We reconstructed orbital changes in the 5 m.y. monsoonal record at Site 758 using time series of *Uvigerina proboscidea* and *Epistominella exigua*. *U. proboscidea* has been suggested to bloom during summer monsoon season[9,12,17], whereas *E. exigua* increases during winter monsoon season[12,24,25]. *U. proboscidea* is a non-oppor-

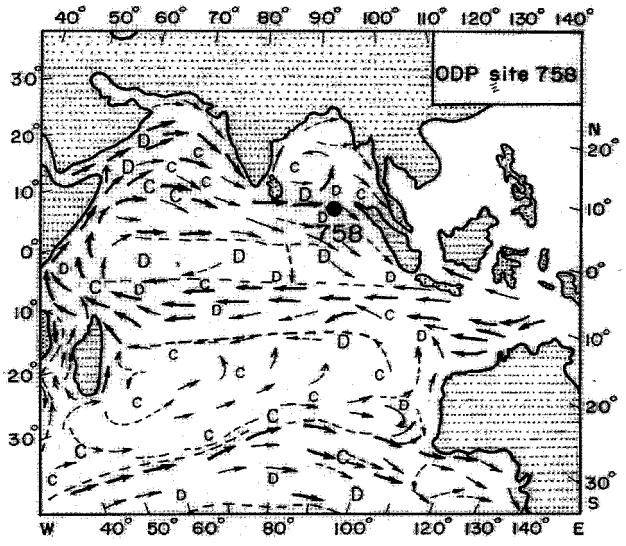

Figure 1. Location of ODP Site 758 in the eastern equatorial Indian Ocean with regard to present-day surface current patterns during the SW monsoon season (boreal summer). C, convergence; D, Divergence.

tunistic intermediate infaunal benthic foraminifer common at bathyal depths that thrives in areas of high surface productivity with sustained flux of organic matter in the Indian[9,12,13], Atlantic[26] and Pacific[27] oceans. These conditions develop during the summer monsoon season. Thus down-core changes in *U. proboscidea* time series have been linked with the summer monsoon variability[9,12,17]. *E. exigua* is a cosmopolitan epifaunal opportunistic species, which thrives in overall oligotrophic conditions with strongly pulsed flux of organic matter to the sea floor[11,24,28,29]. These conditions are produced during the NE monsoon season. Thus changes in *E. exigua* populations could be used to understand winter monsoon variability.

We used continuous wavelet transform (CWT) technique to analyse our signals in the time–frequency domain. The CWT expands the signal into a two-dimensional parameter space and yields a measure of the relative amplitude of local activity at any time and frequency[30]. The CWT therefore enables us to estimate the time–frequency characteristics, such as the amplitude and frequency modulations of the different components of the signals. Generally speaking, the CWT is infinitely redundant, the 1D original signal being transformed in a 2D time–frequency image. Nevertheless, the fundamental information can be extracted from the so-called ridges of the CWT. These ridges consist of continuous lines in the time–frequency representation from which the different deterministic components of the signal can be extracted. The CWT used in this article is described in Mélice *et al.*[31]. Here, we use the ridge procedure described in Delprat *et al.*[32] to filter out the components embedded in the signals. Finally, to perform CWT, the signals must have a regular time spacing interval. Here, the signals are linearly interpolated with 1-kyr resolution before being wavelet-transformed.

Results and discussion

The *U. proboscidea* and *E. exigua* signals are displayed in Figures 2 and 3 from 5000 to 0 kyr BP. Each signal consists of 134 records with uneven time sampling. The time-sampling interval between two successive records is plotted in Figure 4. From 1200 to 0 kyr BP, the sampling interval is smaller than 40 kyr and is rather regular. From 2000 to 1200 kyr BP, it is around 60 kyr and is also quite regular, while before ~2000 kyr BP it is very irregular and mostly larger than ~60 kyr. With such uneven sampling, we have to be careful with interpretation of frequency analyses of the signals, as there is potential for aliasing effects. As a rule of thumb, only the periods about 10 times larger than the sampling interval should be considered as real and non-biased by the aliasing effects. In the last 2000 kyr of our records, the sampling intervals vary from ~30 to ~60 kyr. We can therefore only resolve oscillations with periods larger than about 400 kyr and no physical significance can be attached to any oscillation with shorter periods, although we expect precession and obliquity signals in the record[14]. As a consequence, the

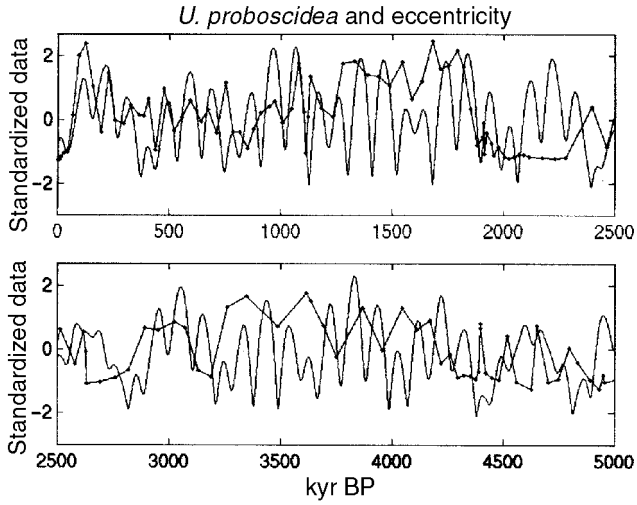

Figure 2. *Uvigerina proboscidea* and eccentricity signals.

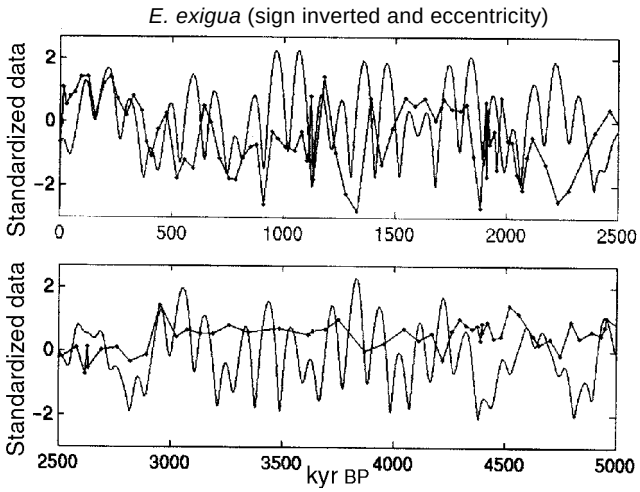

Figure 3. *Epistominella exigua* (sign inverted) and eccentricity signals.

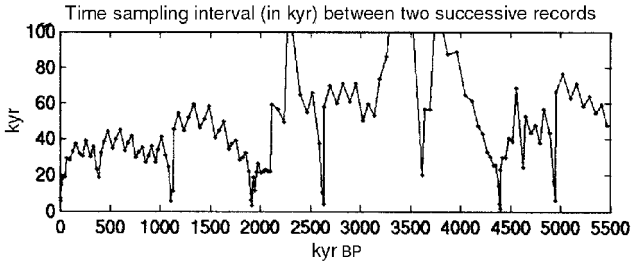

Figure 4. Time-sampling interval (in kyr) between two successive records of the *E. exigua* and *U. proboscidea* signals.

only astronomical parameter that can be explored for an association with the faunal signals is the 400-kyr component of eccentricity.

The eccentricity parameter is superimposed on the faunal signals in Figures 2 and 3. Visually, we can observe some association between the eccentricity and both faunal data in the last ~1500 kyr. This association is explored with more precision after extracting the low-frequency ~400 kyr component of the signals with the CWT and ridge methods (Figures 5 and 6). The CWT is also used to illustrate the aliasing problem in our data. The CWT of the eccentricity signal (with 1 kyr resolution) is displayed in Figure 7 (bottom), where we observe the 100-kyr and the 400-kyr components. The ridge of this last component is superimposed on the CWT image and its corresponding extracted 400-kyr component is plotted against the original data in Figure 7 (top) and also in Figure 8. To illustrate the aliasing effect, we have sampled the eccentricity signal at the same 134 time samplings than the faunal signal (Figure 9, top). We have then interpolated the 134 data with 1-kyr resolution and performed the CWT on the interpolated signal (Figure 9, bottom). We note that the 100-kyr component is more or less correctly retrieved only where the sampling resolution is high, i.e. in the vicinity of 2000, 1000, 500 and 0 kyr BP (Figures 4 and 9). We also note that the 400-kyr component (see the ridge and the extracted component in Figures 8 and 9) is correctly retrieved, except around 3700 kyr BP, where the sampling resolution is very poor.

In order to illustrate more clearly the capacity of the CWT to extract correctly any potential 400-kyr-like component embedded in our faunal data, we have performed the same exercise with the more complex ETP signal. This signal is composed of the sum of the normalized eccentricity, obliquity (tilt) and sign inverted precession signals. The ETP curve is sometimes used as an artificial insolation target curve to which palaeoclimatic records are compared[33]. The CWT of the ETP is displayed in Figure 10. The CWT image and the extracted

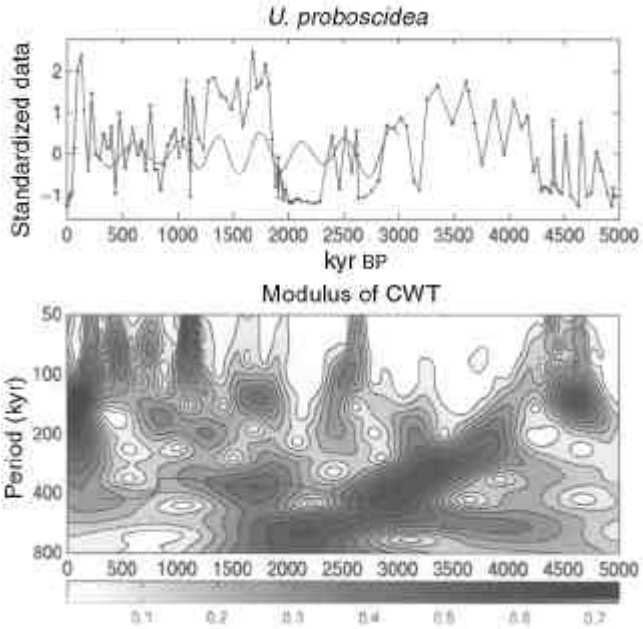

Figure 6. (Top) *U. proboscidea* and its ~400-kyr component. (Bottom) CWT modulus and ~400-kyr ridge (thick line) of *U. proboscidea* signal.

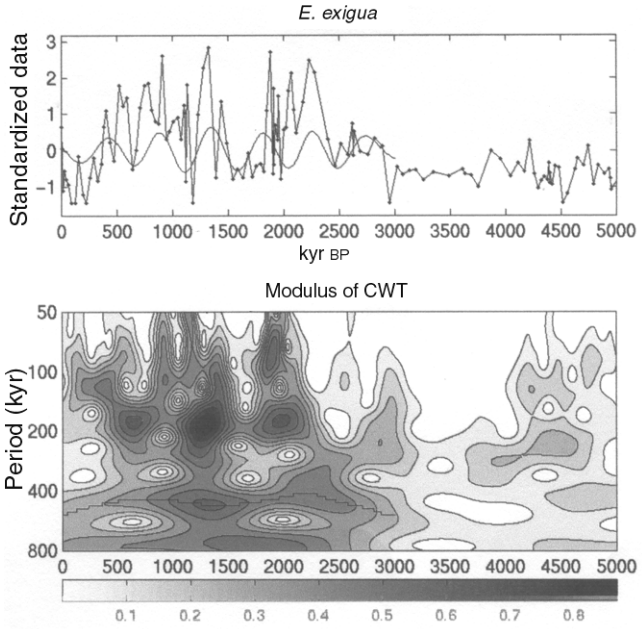

Figure 5. (Top) *E. exigua* and its ~400-kyr component. (Bottom) CWT modulus and ~400-kyr ridge (thick line) of *E. exigua* signal.

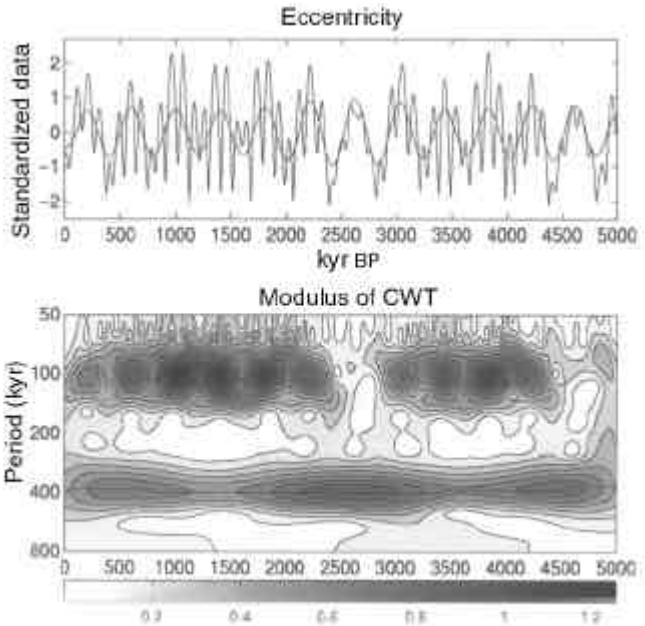

Figure 7. (Top) Eccentricity and its ~400-kyr component. (Bottom) CWT modulus and ~400-kyr ridge (thick line) of the eccentricity signal.

400-kyr component correspond to those of the eccentricity (Figures 7 and 8). The CWT of the ETP, sampled at the 134 time sampling intervals of the faunal data and interpolated at 1-kyr, is displayed in Figure 11. We note that the 100-kyr component is completely distorted by the aliasing effects: it mainly disappears in the last 1500-kyr of the record and spurious ~200-kyr components are produced. We also note that the 400-kyr component is correctly retrieved and may be compared to one of the eccentricity signals (Figures 7 and 8). The 400-kyr components extracted from the original and sampled eccentricity and ETP signals are plotted in Figure 8. The phase and amplitude modulation of the different 400-kyr components are in good agreement with those of the 400-kyr eccentricity component. This demonstrates that the CWT method used to extract the 400-kyr component is physically grounded and that any low-frequency oscillation with a period around 400-kyr that will be extracted from the unevenly sampled *E. exigua* and *U. proboscidea* signals is not an artifact.

The CWT of the *E. exigua* signal (Figure 5) indicates a low-frequency component, with a period around 400-kyr. The corresponding ridge is superimposed on the CWT

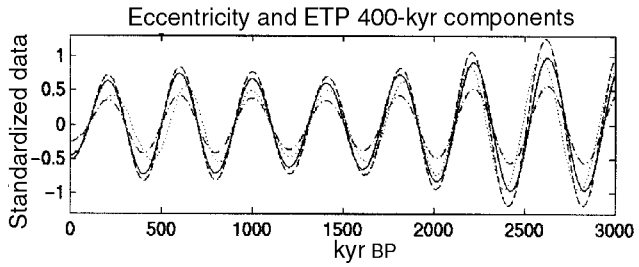

Figure 8. CWT-extracted 400-kyr components of raw eccentricity (solid curve), sampled eccentricity (dashed curve), raw ETP (dash-dotted curve), and sampled ETP (dotted curve) signals.

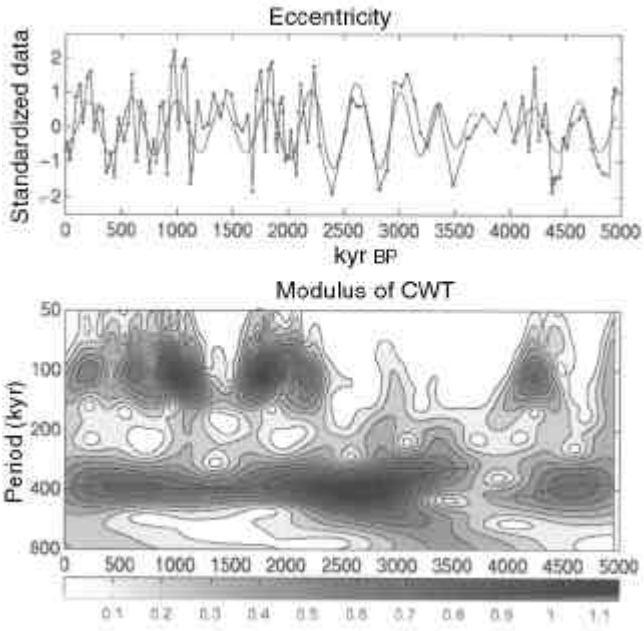

Figure 9. (Top) Eccentricity (sampled at time sampling intervals of *E. exigua* and *U. proboscidea* signals) and its ~400-kyr component. (Bottom) CWT modulus and ~400-kyr ridge (thick line) of the sampled eccentricity signal.

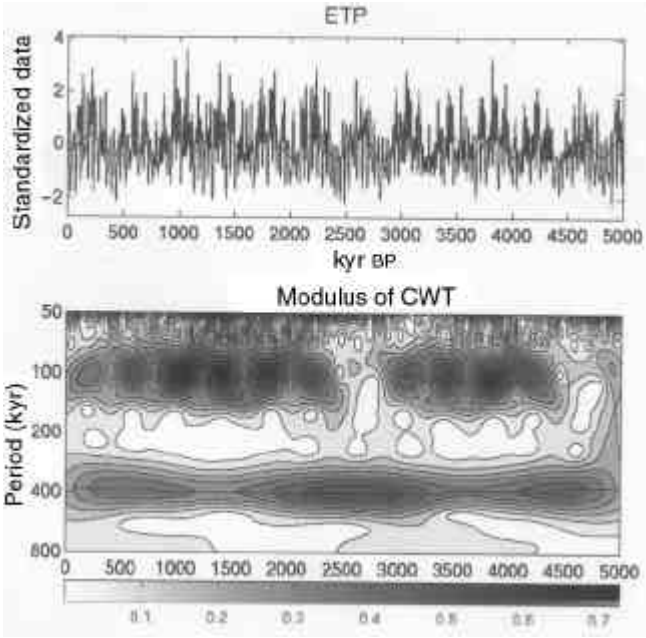

Figure 10. (Top) ETP and its ~400-kyr component. (Bottom) CWT modulus and ~400-kyr ridge (thick line) of the ETP signal.

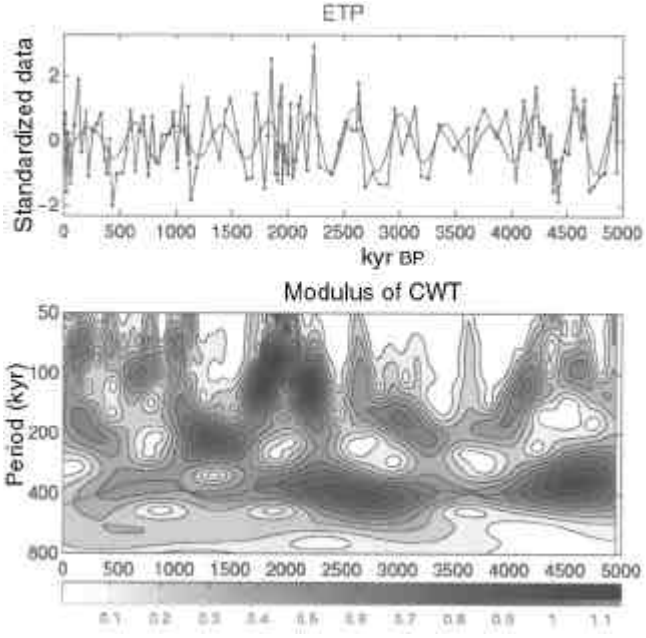

Figure 11. (Top) ETP (sampled at time sampling intervals of *E. exigua* and *U. proboscidea* signals) and its ~400-kyr component. (Bottom) CWT modulus and ~400-kyr ridge (thick line) of the sampled ETP signal.

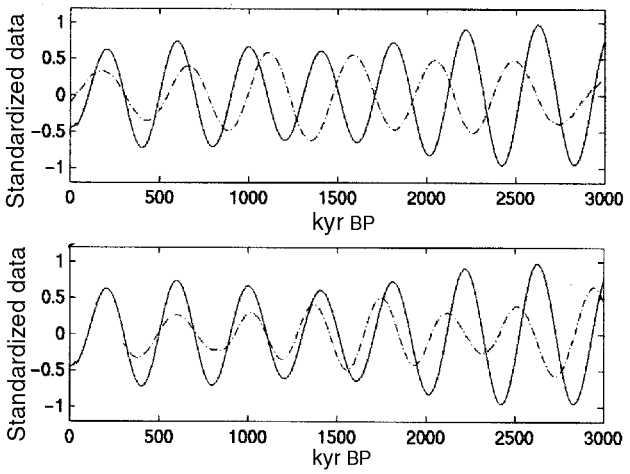

Figure 12. (Top) CWT-extracted eccentricity (solid curve) and sign inverted *E. exigua* (dash-dotted curve) ~400-kyr components. (Bottom) CWT-extracted eccentricity (solid curve) and *U. proboscidea* (dash-dotted curve) ~400-kyr components.

image (bottom), and the component is plotted on the original signal (top). It is also plotted with inverted sign against the 400-kyr component of eccentricity in Figure 12. The two components show an inverse phase relation during the last ~700 kyr. The CWT of the *U. proboscidea* signal is displayed in Figure 6, showing the presence of a 400-kyr component. The corresponding ridge is superimposed on the CWT image (Figure 6, bottom), and the 400-kyr component is plotted against the signal (Figure 6, top) and also in Figure 12. The *U. proboscidea* time series is in phase with the 400-kyr component of the eccentricity during the past ~1700 kyr (Figure 12).

This study shows an inverse relation between the raw data of *U. proboscidea* and *E. exigua*, representing two different seasons of the Indian monsoon. Such inverse relation is also observed during the past ~1000 kyr in the CWT-extracted 400-kyr components (Figure 12). The variable relation between the monsoon proxies and earth's eccentricity at Site 758 agrees with the argument by Bloemendal and de Menocal[20] that orbital forcing of the Indian monsoon shows major shifts during the Plio-Pleistocene. These shifts correspond to the advent of growth and decay of the Northern Hemisphere ice sheets since the last 2.5 Ma[20]. We could not identify precessional and obliquity cycles in the Indian monsoon because of low sampling interval in our study. The sample density was kept low because of the time-frame of the project and samples were procured for different purposes. Nevertheless, we identified the 400-kyr component of the eccentricity in our signals, which has been observed earlier[17].

1. Webster, P. J., in *The Elementary Monsoon* (eds Fein, J. S. and Stephens, P. L.), John Wiley, New York, 1987, pp. 3–32.
2. Clemens, S. C., Prell, W. L., Murray, D., Shimmield, G. and Weedon, G., *Nature*, 1991, **353**, 720–725.
3. Hastenrath, S. and Lamb, P. J., *Climatic Atlas of the Indian Ocean. I: Surface Climate and Atmospheric Circulation*, University of Wisconsin Press, Madison, 1979, pp. 1–116.
4. Radhakrishna, B. P., in *Vedic Sarasvati* (eds Radhakrishna, B. P. and Merh, S. S.), Geological Society of India, 1999, Mem. 42, 1999, pp. 5–13.
5. de Menocal, P., *Science*, 1995, **270**, 53–59.
6. Prell, W. L., in *Climate Processes and Climate Sensitivity* (eds Hansen, J. E. and Takahashi, T.), American Geophysical Union, Washington, 1984, pp. 48–57.
7. Anderson, D. M. and Prell, W. L., *Paleoceanography*, 1993, **8**, 193–208.
8. Hermelin, J. O. R., in *Upwelling Systems: Evolution Since the Early Miocene* (eds Summerhays, C. E. P. *et al.*), Geological Society of London, Special Publication, 1992, vol. 64, pp. 151–166.
9. Gupta, A. K. and Srinivasan, M. S., *Mar. Micropaleontol.*, 1992, **19**, 355–367.
10. Gooday, A. J., *Palaios*, 1994, **9**, 14–41.
11. Smart, C. W., King, S. C., Gooday, A. J., Murray, J. W. and Thomas, E., *Mar. Micropaleontol.*, 1994, **23**, 89–99.
12. Gupta, A. K. and Thomas, E., *Paleoceanography*, 1999, **14**, 62–73.
13. Almogi-Labin, A., Schmiedl, G., Hemleben, C., Siman-Tov, Segl, M. and Meischner, D., *Mar. Micropaleontol.*, 2000, **40**, 295–319.
14. Clemens, S. C., Murray, D. W. and Prell, W. L., *Science*, 1996, **274**, 943–948.
15. Beaufort, L., Lancelot, Y., Camberlin, P., Cayre, O., Vincent, E., Bassinot, F. and Labeyrie, L., *Science*, 1997, **278**, 1451–1454.
16. Altabet, M. A., Murray, D. W. and Prell, W. L., *Paleoceanography*, 1999, **14**, 732–743.
17. Gupta, A. K., Dhingra, H., Mélice, J.-L. and Anderson, D. M., *Geophys. Res. Lett.*, 2001, **28**, 413–4134.
18. Prell, W. L. and Kutzbach, J. E., *Nature*, 1992, **360**, 647–652.
19. Rutherford, S. and D'Hondt, S., *Nature*, 2000, **408**, 72–75.
20. Bloemendal, J. and de Menocal, P., *Nature*, 1989, **342**, 897–900.
21. Peirce, J. *et al.*, Proceedings of the Ocean Drilling Programme, 1989, vol. 121, pp. 359–453.
22. Berggren, W. A., Kent, D. V. and Van Couvering, J. A., *Spec. Publ. Soc. Econ. Paleontol. Mineral.*, 1995, **54**, 129–212.
23. Schott, F. A. and McCreary, J. P., Jr., *Prog. Oceanogr.*, 2001, **51**, 1–123.
24. Gooday, A. J., *Mar. Micropaleontol.*, 1993, **22**, 187–205.
25. Gupta, A. K., *J. Foram. Res.*, 1997, **27**, 196–208.
26. Thomas, E., Booth, L., Maslin, M. A. and Shackleton, N. J., *Paleoceanography*, 1995, **10**, 545–562.
27. Woodruff, F., *Geol. Soc. Am. Mem.*, 1985, **163**, 131–176.
28. Mackensen, A., Schniedl, G., Harloff, J. and Giese, M., *Micropaleontology*, 1995, **41**, 342–358.
29. Ohkushi, K., Thomas, E. and Kawahata, H., *Mar. Micropalentol.*, 2000, **38**, 119–147.
30. Torrence, C. and Compo, J. P., *Bull. Am. Meteorol. Soc.*, 1998, **79**, 61–78.
31. Mélice, J.-L., Coron, A. and Berger, A. L., *J. Climate*, 2001, **14**, 1043–1054.
32. Delprat, N., Escuidé, B., Guillemain, P., Kronland-Martinet, R., Tchamitchian, P. and Torrésani, B., *IEEE Trans. Inf. Theory*, 1992, **38**, 644–664.
33. Imbrie, J. *et al.*, in *Milankovitch and Climate, Part 1* (eds Berger, A. L. *et al.*), NATO ASI Series, Reidel, Dordrecht, 1984, pp. 269–305.

Received 29 July 2002; revised accepted 23 April 2003